Newsletter #43- 2007

ON THE ACCURACY OF INTENSITY FACTORS IN CRACKED PIEZOELECTRIC MATERIALS COMPUTED BY THE FINITE ELEMENT METHOD

Leslie Banks-Sills, Yael Motola and Lucy Shemesh
The Dreszer Fracture Mechanics Laboratory
Faculty of Engineering
Tel Aviv University
69978 Ramat Aviv, Israel

Abstract Piezoceramic elements can be manufactured easily in large quantities and in specific shapes. This makes them ideally suited for adaptive structural applications in the form of actuators, sensors, controllers and transducers. When employed in this way, piezoelectric ceramics are subjected to complex behavior associated with interactions between their mechanical and electrical fields. Since these ceramics are rather brittle and may crack during use, reliability and failure behavior of piezoelectric materials are important. This leads to the necessity to develop techniques for predicting crack growth under monotonic and fatigue loading (both mechanical and electric). To this end, accurate methods are required for calculating stress and energy flux density intensity factors in these materials. The solution is affected by the mechanical and electrical coupling, as well as material anisotropy in its poled state. In this study, the accuracy of the M-integral in calculating intensity factors is demonstrated with some example problems. In addition, some results are obtained with the displacement/potential extrapolation method.

1. Introduction

As a result of their wide use in the form of sensors and actuators, much interest has been focused on the reliability and failure behavior of piezoelectric materials. This leads to the necessity to develop techniques for predicting crack growth under monotonic and fatigue loading (both mechanical and electric). To this end, accurate methods are required for calculating stress and energy flux density intensity factors in these materials. The solution is affected by the mechanical and electrical coupling, as well as material anisotropy in its poled state.

Methods for calculating stress intensity factors from numerical calculations, such as the finite element method, for mechanically loaded cracked bodies have been presented in many studies (see for example [1]). The area M-integral and displacement/potential extra-polation method for impermeable crack face boundary conditions were presented and employed to obtain intensity factors for cracks in piezoelectric materials in [2]. In this study, the accuracy of these methods is examined.

One form of the constitutive equations is given by

$$\begin{aligned} \sigma_{ij} &= C^{E}_{ijkl}\varepsilon_{kl} + e_{sij}E_s \\ D_i &= e_{ikl}\varepsilon_{kl} + \kappa^{\varepsilon}_{is}E_s \end{aligned} \qquad (1)$$

where i,j,k,l,s = 1,2,3. The stress and strain components are denoted by σ_{ij} and ε_{ij}, respectively; the electric flux density and the electric field components are given by D_i and E_i, respectively. The material properties are the stiffness tensor C^{E}_{ijkl} where the superscript E denotes that $\boldsymbol{C}$ is measured with the electric field held constant, the piezoelectric coupling coefficient e_{ikl} and the permittivity $\kappa^{\varepsilon}_{is}$ where the superscript $\boldsymbol{\varepsilon}$ indicates that $\boldsymbol{\kappa}$ is measured with the strain held constant. Coupling between the mechanical and electric behavior of the material may be observed in eqs. (1).

The M-integral is given by [2]

$$M^{(1,2\alpha)} = \int_A \left[\hat{C}_1^{(1,2\alpha)} - \hat{C}_2^{(1,2\alpha)} + \hat{h}^{(1,2\alpha)}\delta_{1\beta}\right]\frac{\partial q_1}{\partial \hat{x}_\beta}\,d\hat{A} \qquad (2)$$

where the superscript (1) represents the sought after solution and the superscript (2α) represents auxiliary solutions with $\alpha = a,b,c,d$. In eq. (2),

$$\hat{C}_1^{(1,2\alpha)} = \hat{T}_\beta^{(1)}\hat{u}_{\beta,1}^{(2\alpha)} + \hat{T}_\beta^{(2\alpha)}\hat{u}_{\beta,1}^{(1)} \qquad (3)$$

$$\hat{T}_\beta = \hat{\sigma}_{\beta 1}n_1 + \hat{\sigma}_{\beta 2}n_2 \qquad (4)$$

$\beta = 1,2$, **n** is the outward normal to the area A in which the integral in eq. (2) is carried out. The hat above a quantity indicates that it is normalized (see [2] for a full explanation). The normalized stress components are $\hat{\sigma}_{\beta\gamma}$ ($\gamma = 1,2$), $\hat{u}_\beta$ represents the normalized displacement components and a comma represents differentiation. In eq. (2),

$$\hat{C}_2^{(1,2\alpha)} = c_3\left[\hat{D}_\beta^{(1)} n_\beta \hat{E}_1^{(2\alpha)} + \hat{D}_\beta^{(2\alpha)} n_\beta \hat{E}_1^{(1)}\right] \qquad (5)$$

where $\hat{D}_\beta$ and $\hat{E}_1$ are the normalized electric flux density components and electric field component in the x-direction, respectively. Equations (2) through (5) are written in the crack tip coordinates shown in Fig. 1. In eq. (5),

$$c_3 = \frac{e_{26}^2}{\kappa_{22} E_A} \qquad (6)$$

where e_{26} is a component of the piezoelastic coupling contracted tensor, κ_{22} is a component of the permittivity tensor and E_A is the Young's modulus in the axial material direction. In eq. (2),

$$\hat{h}^{(1,2\alpha)} = \hat{\sigma}_{\beta\gamma}^{(1)} \hat{\varepsilon}_{\beta\gamma}^{(2\alpha)} - c_3 \hat{D}_\beta^{(1)} \hat{E}_\beta^{(2\alpha)} \qquad (7)$$

is the normalized electric enthalpy density, δ is the Kronecker delta, q_1 is the normalized virtual crack extension, and $\hat{A} = A / L^2$ with L a characteristic length.

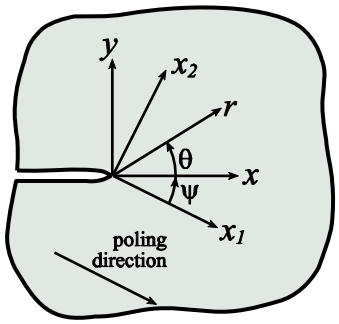

Fig. 1 – Crack tip and material coordinates.

Calculation of the M-integral is carried out in a ring of elements surrounding the crack tip as shown in Fig. 2.

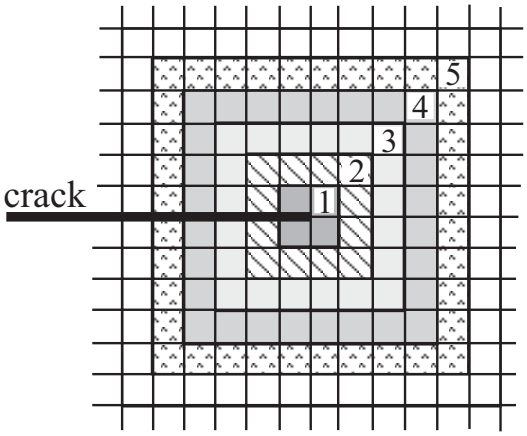

Fig. 2 - Mesh and integration regions about the crack tip.

On the other hand, it was shown in [2] that

$$M^{(1,2\alpha)} = \frac{1}{2}\left[\left(\hat{\mathbf{k}}^{(1)}\right)^T \hat{\mathbf{L}}^{-1} \hat{\mathbf{k}}^{(2\alpha)} + \left(\hat{\mathbf{k}}^{(2\alpha)}\right)^T \hat{\mathbf{L}}^{-1} \hat{\mathbf{k}}^{(1)}\right] \qquad (8)$$

where $\hat{\mathbf{k}}$ is the normalized intensity factor vector

$$\hat{\mathbf{k}}^T = \left[\hat{K}_{II}\ \hat{K}_I\ \hat{K}_{III}\ \hat{K}_{IV}\right] \qquad (9a)$$

with

$$\hat{K}_{I/II} = \frac{K_{I/II}}{E_A\sqrt{L}},\ \hat{K}_{III} = \frac{K_{III}}{G_A\sqrt{L}},\ \hat{K}_{IV} = \frac{K_{IV}}{e_{26}\sqrt{L}} \qquad (9b)$$

the superscript T represents the transpose of the vector, $\hat{\mathbf{L}}$ is one of the 4×4 normalized Barnett-Lotte tensors and is a function of material properties, and G_A is the shear modulus in the axial material direction. Normalization is carried out so that the diagonal and off-diagonal elements of $\mathbf{L}$ are of the same order of magnitude (see [2] for details).

To obtain the intensity factors $K_I^{(1)}$, $K_{II}^{(1)}$, $K_{III}^{(1)}$ and $K_{IV}^{(1)}$, four auxiliary solutions are chosen, namely $2a$, $2b$, $2c$ and $2d$. The first term of the asymptotic solution is used with the intensity factors given in Table 1.

Table 1 – Intensity factor values for the auxiliary solutions 2α.

	K_I	K_{II}	K_{III}	K_{IV}
$2a$	1	0	0	0
$2b$	0	1	0	0
$2c$	0	0	1	0
$2d$	0	0	0	1

Equating eqs. (2) and (8) allows determination of the desired intensity factors.

2. Numerical Results

In this section, both the extrapolation and M-integral methods are employed to calculate intensity factors for impermeable cracks in piezoelectric material. For these applications, the finite element program ANSYS [3] is used to obtain the displacement field and the electric potential. The elements exploited here are isoparametric, containing eight nodal points for the in-plane problems and twenty nodes for the mode III problems. Singular, quarter-point square and cubic elements are used at the crack tip and front, respectively.

For the in-plane problems, both extrapolation and the M-integral are utilized. Since a three-dimensional version of the M-integral is required for analysis of the mode III problems, only the former method is employed. The M-integral is evaluated in rings surrounding the crack tip. The five rings used in this study are shown in Fig. 2. The numbers designate the rings.

In the calculations, it was observed that the results in path 1 produced less accurate results. In addition, sometimes there were small differences in path 2. The results shown in the sequel are an average of paths 3 through 5. Some details will be shown in Section 2.2 for the two-dimensional problems.

For the extrapolation method, a 'best' straight line is passed through successive groups of points in the vicinity of the crack tip. The result is chosen for which the correlation coefficient is closest to unity.

The material used in this study to illustrate the methods is PZT-5H from Morgan Electro Ceramics [4] with the properties presented in Table 2. The poling direction is along the x_1-axis.

Table 2 – Material properties for PZT-5H from [4].

property	C_{11}^E (GPa)	C_{22}^E (GPa)	C_{55}^E (GPa)
value	117	126	23.0
property	C_{12}^E (GPa)	C_{23}^E (GPa)	
value	84.1	79.5	
property	e_{11} (C/m^2)	e_{12} (C/m^2)	e_{26} (C/m^2)
value	23.3	-6.55	17.0
property	$\kappa_{11}^{\varepsilon}$ (F/m)	$\kappa_{22}^{\varepsilon}$ (F/m)	
value	1.3×10^{-8}	1.5×10^{-8}	

In Section 2.1, a benchmark problem is presented for the case in which the poling direction is parallel to the crack front. The first term of the asymptotic solution for the displacement field and electric potential is used as a boundary condition on the outer boundary of a disk. Intensity factors are prescribed which should be obtained as the solution to the calculations. This is a check on the fields and numerical calculations, as well as the mesh density. Next in Section 2.2, several in-plane problems are solved with poling taken at an angle to the the crack faces as shown in Fig. 1. Two problems are solved: the benchmark problem and a finite crack in an infinite body. For all cases, traction and normal energy flux density free boundary conditions are imposed on the crack faces. This implies impermeable crack conditions.

2.1 Poling direction parallel to the crack front

In this section, the poling direction is taken to be along the x_3-axis. The material properties in Table 2 are rotated appropriately. The crack front direction is along the z-axis; these axes coincide. For this problem, the out-of-plane deformation and the in-plane electric field are coupled. Hence, modes III and IV are studied in this section.

In the first problem considered, the first term in the asymptotic expansion for the displacement field and electric potential are applied to the outer boundary of a disk containing an edge crack (see Fig. 3). Various combinations of intensity factors are imposed; the solution should duplicate these enforced intensity

factors. This is defined as the benchmark problem. In Fig. 3, the normalized crack length $a/R=1$ and the normalized thickness $B/R=0.03$.

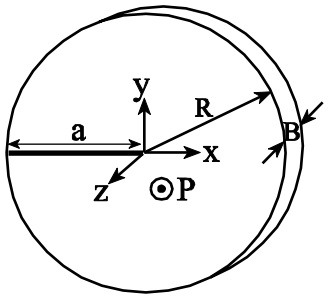

Fig. 3 - Benchmark problem of a disk containing an edge crack.

Two finite element meshes were constructed as shown in Fig. 4; these are the in-plane meshes. The quarter-point elements along the crack front are cubic. This leads to the best simulation of the square-root singularity for a brick element. The elements along the crack front for the fine mesh have a height, width, thickness ratio of 1:1:10. For the coarse mesh, the ratio is 1:1:5.

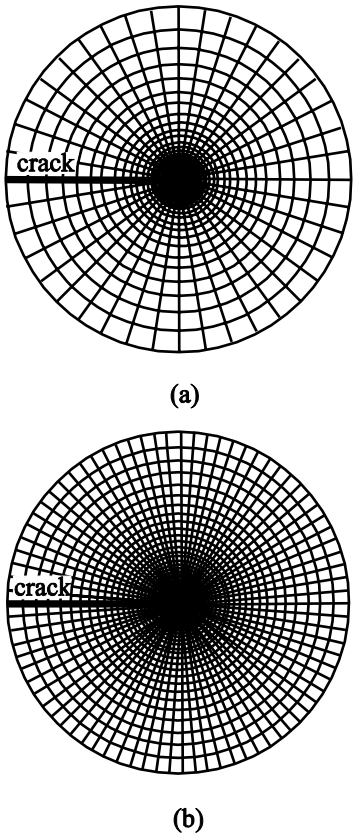

Fig. 4 - In-plane meshes for the disk in Fig. 3.

(a) Coarse mesh containing 3,900 brick elements and 20,112 nodal points. (b) Fine mesh containing 12,000 brick elements and 61,052 nodal points.

For each mesh there are three elements through the thickness. Details of the meshes near the crack tip are exhibited in Fig. 5. For the coarse mesh in Fig. 5a, the ratio of an element side in the plane to the crack length is $\ell/a=2\cdot10^{-3}$. For the fine mesh in Fig. 5b, this ratio is half of that of the coarse mesh.

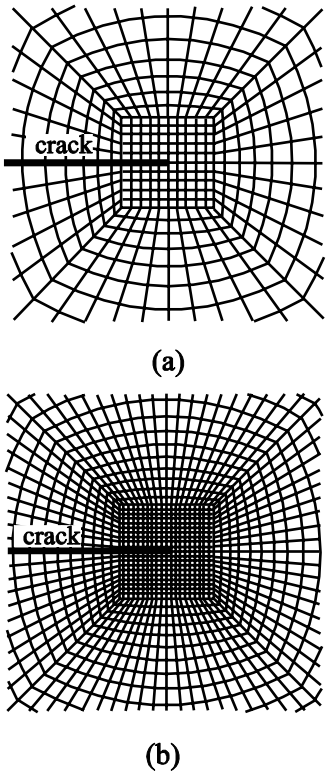

Fig. 5 - Meshes in the neighborhood of the crack tip. (a) Coarse mesh; crack tip element size is $\ell/a=2\cdot10^{-3}$. *(b) Fine mesh; crack tip element size is* $\ell/a=1\cdot10^{-3}$.

The first term of the asymptotic expansions for the displacement $\hat{u}_3$ and the electric potential $\hat{u}_4$ is imposed on the outer boundary of the disk with

$$\hat{K}_{III}=1 \qquad \hat{K}_{IV}=0. \tag{10}$$

The intensity factors are calculated by means of the extrapolation method along one of the rays of the middle element along the crack front. The jump in the displacement and electric potential along the crack faces, normal to the crack front, are obtained from the finite element

results and used to obtain local intensity factors [2]. In the graph obtained by this method for mode III, the first five points closest to the crack front for both the fine and coarse meshes differ greatly from the straight line fit in the neighborhood of the crack tip; for mode IV, the first three points show large differences from the remainder of the points. Neglecting these points, the results are extrapolated to zero and presented in Table 3. The results for both meshes for $\hat{K}_{III}$ are excellent. For $\hat{K}_{IV}$ the results are small. This is the level of zero that is obtained with these meshes. It may be observed that the coarse mesh yields sufficiently accurate results. In fact, a coarser mesh could have been used. Such a mesh will be considered for the analogous in-plane problem in Section 2.2.1.

Table 3 – Calculated intensity factors for the problem in Fig. 3 with the boundary conditions employing eq. (10).

	$\hat{K}_{III}$	$\hat{K}_{IV}$
coarse mesh	0.9998	1.8×10^{-5}
fine mesh	0.9999	9.7×10^{-6}

Next, the intensity factors

$$\hat{K}_{III}=0 \qquad \hat{K}_{IV}=1 \tag{11}$$

are imposed through the boundary conditions on the outer surface of the disk in Fig. 3. The same meshes shown in Fig. 4 were used to calculate the displacement field and electric potential. The intensity factors were calculated by means of extrapolation and are presented in Table 4. The results for both intensity factors deteriorate slightly as compared to those in Table 3. However, those for $\hat{K}_{IV}$ are excellent.

Table 4 – Calculated intensity factors for the problem in Fig. 3 with the boundary conditions employing eq. (11).

	$\hat{K}_{III}$	$\hat{K}_{IV}$
coarse mesh	1.1×10^{-4}	0.9996
fine mesh	-4.9×10^{-5}	0.9995

The problem studied with the two sets of boundary conditions demonstrates that with a refined mesh, intensity factors may be obtained accurately by the extrapolation method and quarter-point elements.

2.2 Poling direction at an angle to the crack faces within the crack plane

In this section, poling is within the xy-plane and at an angle to the crack faces as shown in Fig. 1. Several problems are considered in this section. First, the equivalent disk problem solved in Section 2.1 is reconsidered for this poling direction. Next, intensity factors for a finite length crack in an infinite body subjected to various boundary conditions at infinity are determined. The results are compared to analytic solutions. These problems are chosen to examine the accuracy of the solutions, mesh refinement required, and the differences between the two methods presented.

2.2.1 Benchmark problem

The disk containing an edge crack and shown in Fig. 6 is studied. Poling is chosen such that $\psi=-30^{\circ}$ and the non-dimensional crack length $a/R=1$. The crack faces are traction and energy flux density free. On the outer boundary of the disk, the first term of the asymptotic displacement field and electric potential are enforced with different values for the normalized intensity factors. The three problems considered are $2a$, $2b$, and $2d$ shown in Table 1.

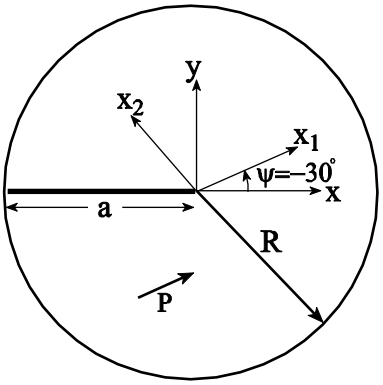

Fig. 6 - In-plane benchmark problem of a disk containing an edge crack.

The coarse and fine meshes are illustrated in Fig. 7. The coarse mesh contains 180 eight noded isoparametric elements and 595 nodal points, whereas the fine mesh contains 900 eight noded isoparametric elements and 2,791 nodal points. The ratio of the crack tip element

length to crack length is $\ell / a = 0.1$ for the coarse mesh and $2 \cdot 10^{-3}$ for the fine mesh. The fine mesh used here is the in-plane mesh that was used as the coarse mesh in Section 2.1 for the three-dimensional problem. Thus, the detail in Fig 5a is appropriate for the mesh in Fig. 7b.

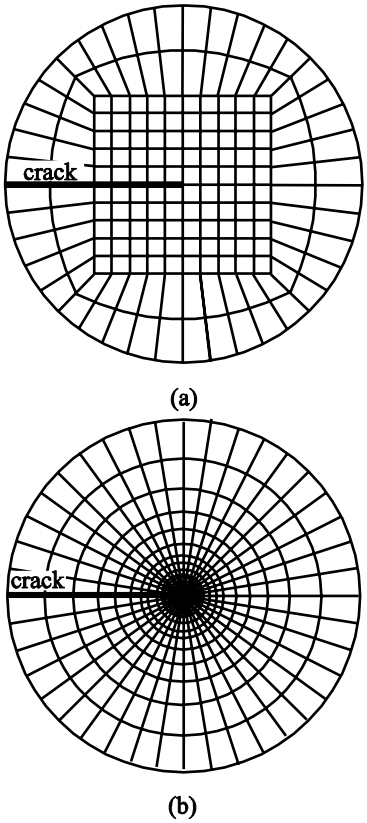

Fig. 7 - Meshes for the disk in Fig. 6. (a) The coarse mesh contains 180 eight noded isoparametric elements and 595 nodal points. (b) The fine mesh contains 900 eight noded isoparametric elements and 2,791 nodal points.

Results are presented in Table 5 for problem $2a$ in Table 1. For the M-integral, the average of results obtained in the three outer paths (3, 4 and 5) in Fig. 2 are given. It is observed that the values of $\hat{K}_I$ for both the coarse and fine meshes are excellent (the value should be unity). There is some deterioration for $\hat{K}_{IV}$ with the coarse mesh. It was seen that even results in paths 1 and 2 are excellent. It may be observed, further, that values obtained by means of the extrapolation method are also in excellent agreement with the prescribed values. The largest discrepancy of $\hat{K}_I$ from unity is 0.3% for extrapolation and the coarse mesh.

Problems $2b$ and $2d$ in Table 1 were also solved. The results are similar to those found for the mode I case (problem $2a$). The largest error of 1.6% for $\hat{K}_{II}$ (problem $2b$) was found with extrapolation and the coarse mesh. It may be noted that in all cases, near the crack tip, the values of displacement and electric potential deviate substantially from unity.

Table 5 - Calculated intensity factors for the problem in Fig. 6 with the boundary conditions for problem $2a$ in Table 1

	$\hat{K}_I$	$\hat{K}_{II}$	$\hat{K}_{IV}$
M-integral			
coarse mesh	1.0004	$O(10^{-5})$	$O(10^{-4})$
fine mesh	1.00002	$O(10^{-6})$	$O(10^{-6})$
extrapolation			
coarse mesh	0.997	$O(10^{-4})$	$O(10^{-3})$
fine mesh	0.999	$O(10^{-4})$	$O(10^{-4})$

.

With the fine mesh in Fig. 7b, poling was taken both parallel ($\psi = 0^\circ$) and perpendicular ($\psi = -90^\circ$) to the crack faces. The same excellent results were obtained for each of the intensity factors which were taken to be unity for both the M-integral and extrapolation methods. In general, the intensity factor that should be zero was found to be between $O(10^{-6})$ and $O(10^{-11})$. An exception occurred when poling was perpendicular to the crack faces and $\hat{K}_I = 1$; $\hat{K}_{IV}$ was found to be $O(10^{-5})$ with the M-integral and $O(10^{-3})$ with extrapolation. Several other results with extrapolation also deteriorated. It is noted that the results for the zero intensity factors for angles different from 0° and -90° (namely, $\psi = -30^\circ$) are for the most part smaller than $O(10^{-8})$.

Although these problems demonstrate the accuracy of the analytically obtained asymptotic fields, as well as the post-processors, they do not demonstrate the strength of the M-integral. To this end, the problem of a Griffith's crack in an infinite body is examined next.

2.2.2 Griffith crack

In this section, a finite length crack in an infinite body illustrated in Fig. 8 is studied. To model an infinite body, the normalized height and crack length are taken, respectively, as $h/W=1$ and $a/W=0.05$. For $a/W=0.1$, the body is not sufficiently infinite. The applied far field boundary conditions include $\sigma_{yy}=\sigma_{\infty}=1\,\text{MPa}$, $\sigma_{xy}=\tau_{\infty}=1\,\text{MPa}$ and $D_y=D_{\infty}=0.01\,\text{C/m}^2$. These boundary conditions are applied in turn. Poling is taken such that $\psi=-30^{\circ}$ (see Fig. 1). The solution to the infinite body problem is [5]

$$K_I=\sigma_{\infty}\sqrt{\pi a},\ K_{II}=\tau_{\infty}\sqrt{\pi a},\ K_{IV}=D_{\infty}\sqrt{\pi a} \tag{12}$$

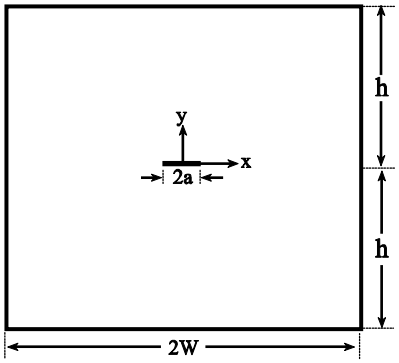

Fig. 8 – Central crack in an infinite body.

As with the previous problems, two meshes were employed. The coarse and fine meshes are illustrated in Figs. 9a and 9b, respectively, with details surrounding the crack tips shown in Fig. 10.

With the M-integral and extrapolation, the intensity factors normalized as in eq. 9b are computed. These are normalized again to yield

$$\tilde{K}_I=\frac{K_I}{\sigma_{\infty}\sqrt{\pi a}},\ \tilde{K}_{II}=\frac{K_{II}}{\tau_{\infty}\sqrt{\pi a}},\ \tilde{K}_{IV}=\frac{K_{IV}}{D_{\infty}\sqrt{\pi a}}. \tag{13}$$

To examine path independence of the M-integral, the mode II problem in which σ_{xy} is applied to the infinite body is considered in detail. It may be observed in Table 6 that the normalized stress intensity factor $\tilde{K}_{II}$ is path independent to five significant figures along paths 2 through 5 (see Fig. 2) for the coarse mesh and paths 3 through 5 for the fine mesh. With σ_{yy} applied, path independence to five significant figures occurred in paths 2 through 5 for the coarse mesh and 3 through 5 for the fine mesh. When D_y was applied there was five significant figure agreement on paths 2 through 5. This occurred for both meshes.

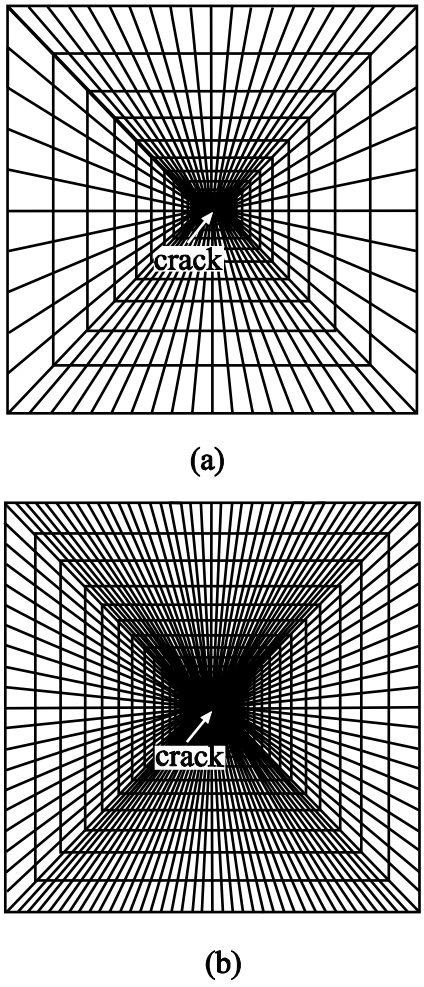

Fig. 9 - Meshes for the plate in Fig. 8. (a) The coarse mesh contains 800 eight noded isoparametric elements and 2,480 nodal points. (b) The fine mesh contains 2,600 eight noded isoparametric elements and 7,960 nodal points.

Table 6 - The stress intensity factor $\tilde{K}_{II}$ along various paths for the problem in Fig. 8 with σ_{xy} applied.

path	coarse mesh	fine mesh
1	1.0016	1.0018
2	1.0005	1.0009
3	1.0005	1.0007
4	1.0005	1.0007
5	1.0005	1.0007

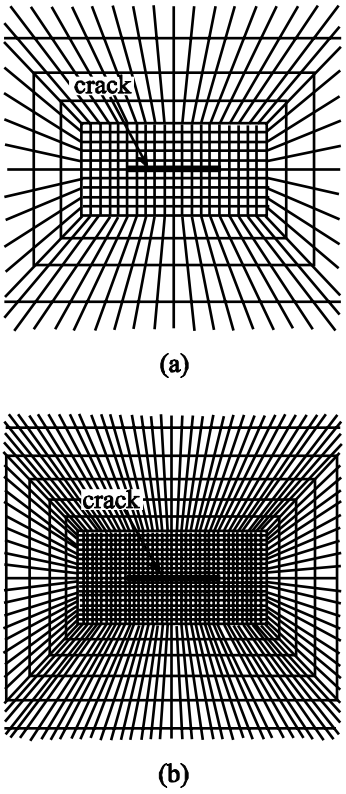

Fig. 10 - Meshes in the neighborhood of the crack tip for the infinite plate. (a) Coarse mesh; crack tip element size is $\ell / a = 0.2$. *(b) Fine mesh; crack tip element size is* $\ell / a = 0.1$.

In Table 7, normalized intensity factors are presented for each of the boundary conditions. It should be noted that both $\tilde{K}$ and $\hat{K}$ defined in eqs. (13) and (9b), respectively, are given for different cases. Values calculated by means of the M-integral are averaged from paths 3 through 5. For mode I deformation, $\tilde{K}_I$ is seen to be the same for the coarse and fine meshes and to differ from the analytic value of unity by 0.4% when calculated by means of the conservative integral. With extrapolation, an error of 1% occurs for the coarse mesh and 0.7% for the fine mesh. When σ_{xy} is applied, $\tilde{K}_{II}$ differs with the expected solution by 0.05% and 0.07%, for the coarse and fine meshes, respectively. Note that the value deteriorates to 1.6% when obtained by extrapolation and the coarse mesh. There is improvement with the fine mesh. Similar results are found when the electric flux density D_y is applied far from the crack. With this example, the superiority of the conservative integral is seen. The values for the intensity factors obtained with the M-integral are observed to be more accurate than those found by means of the extrapolation method. It may be noted, that the coarse mesh is sufficient to obtain extremely accurate results when the M-integral is used in the calculations. In addition, the intensity factors which should be obtained as zero are also presented. When K_I and K_{II} are the dominant stress intensity factors respectively, $\tilde{K}_{II}$ and $\tilde{K}_I$, respectively, are obtained by normalizing with σ_∞ and τ_∞. This is the opposite from that in eq. (13). These values are seen to range between $O(10^{-2})$ and $O(10^{-5})$. If the $\hat{K}_{I/II}$ values are considered instead, they decrease to $O(10^{-7})$ and $O(10^{-9})$. This gives the reader a handle on the level of zero which may be obtained with these methods. Moreover, since $D_\infty = 0$ in these two cases, only $\hat{K}_{IV}$ can be calculated. It is seen to range from $O(10^{-7})$ and $O(10^{-8})$.

Table 7 - Calculated intensity factors for the Griffith crack (see Fig. 8) with various boundary conditions

applied tensile stress	$\tilde{K}_I$	$\tilde{K}_{II}$	$\hat{K}_{IV}$
M-integral			
coarse mesh	1.004	$O(10^{-5})$	$O(10^{-8})$
fine mesh	1.004	$O(10^{-5})$	$O(10^{-8})$
extrapolation			
coarse mesh	1.010	$O(10^{-3})$	$O(10^{-7})$
fine mesh	1.007	$O(10^{-3})$	$O(10^{-8})$
applied shear stress	$\tilde{K}_I$	$\tilde{K}_{II}$	$\hat{K}_{IV}$
M-integral			
coarse mesh	$O(10^{-2})$	1.0005	$O(10^{-7})$
fine mesh	$O(10^{-2})$	1.0007	$O(10^{-7})$
extrapolation			
coarse mesh	$O(10^{-2})$	1.016	$O(10^{-7})$
fine mesh	$O(10^{-2})$	1.007	$O(10^{-7})$
applied electric flux density	$\hat{K}_I$	$\hat{K}_{II}$	$\tilde{K}_{IV}$
M-integral			
coarse mesh	$O(10^{-6})$	$O(10^{-7})$	1.0007
fine mesh	$O(10^{-6})$	$O(10^{-7})$	1.0009
extrapolation			
coarse mesh	$O(10^{-5})$	$O(10^{-5})$	1.016
fine mesh	$O(10^{-6})$	$O(10^{-6})$	1.007

3. Conclusions

The accuracy of a conservative M-integral has been examined for calculating intensity factors of impermeable cracks in piezoelectric materials. Comparisons were made to the extrapolation method. Two geometries were examined: (1) a benchmark problem and (2) a Griffith crack. It was seen that excellent results may be obtained with the M-integral. There was some deterioration with extrapolation.

In the future, the M-integral will be extended and results presented for more realistic crack face boundary conditions.

References

[1] Banks-Sills, L. (1991) Application of the finite element method to linear elastic fracture mechanics, *Applied Mechanics Reviews* **44**, pp. 447-461.

[2] Banks-Sills, L., Motola, Y. Shemesh, L. (2007) The M-integral for calculating intensity factors of an impermeable crack in a piezoelectric material, to appear: *Engineering Fracture Mechanics.*

[3] ANSYS (2004) Release 8.1, Ansys, Inc., Canonsburg, Pennsylvania,.

[4] Berlincourt, D., Krueger, H.A. (1959) Properties of Morgan Electro Ceramic Ceramics. Technical Publication TP-226. Morgan Electro Ceramics.

[5] Pak, Y.E. (1992) Linear electro-elastic fracture mechanics of piezoelectric materials. *International Journal of Fracture* **54**, pp. 79-100.